Accepted Manuscript

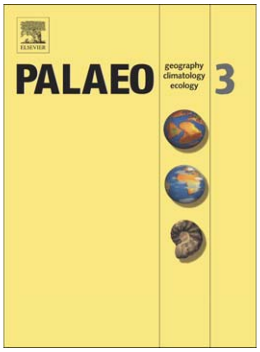

Mid-Holocene regional reorganization of climate variability: Analyses of proxy data in the frequency domain

K.W. Wirtz, G. Lohmann, K. Bernhardt, C. Lemmen

PII: S0031-0182(10)00589-4
DOI: doi: 10.1016/j.palaeo.2010.09.019
Reference: PALAEO 5540

To appear in: *Palaeogeography*

Received date: 26 May 2010
Revised date: 20 September 2010
Accepted date: 21 September 2010

Mid-Holocene regional reorganization of climate variability: Analyses of proxy data in the frequency domain

K. W. Wirtz [a] G. Lohmann [b] K. Bernhardt [a] C. Lemmen [a]

[a] *GKSS Research Center Geesthacht, Institute for Coastal Research, Max-Planck Straße 1, 21501 Geesthacht, Germany*

[b] *Alfred Wegener Institute for Polar and Marine Research, Bussestr. 24, 27483 Bremerhaven, Germany*

Abstract

Recurrent shifts in Holocene climate define the range of natural variability to which the signatures of human interference with the Earth system should be compared. Characterization of Holocene climate variability at the global scale becomes increasingly accessible due to a growing amount of paleoclimate records for the last 9 000–11 000 years. Here, we integrate 124 proxy time series of different types (e.g., δ^{18}O, lithic composition) and apply a modified Lomb-Scargle spectral analysis. After bootstrapping the data in moving time windows we observe an increased probability for generation or loss of periodic modes at the mid-Holocene. Spatial autocorrelation of spectral changes robustly reveals that this (in)activation of modes was organized in regional clusters of subcontinental size. Within these clusters, changes in spectral properties are unexpectedly homogeneous, despite different underlying climatological variables. Oscillations in the climate system were amplified especially at the upwelling areas and dampened in the North Atlantic. We cross-checked the spectral analysis by counting events in the time series and tested against possible dating errors in individual records or against an overestimation of singular events. A combination of different mechanisms may have affected the coupling intensity between climate subsystems, turning these more or less prone to oscillations.

Key words: Holocene, Regional patterns, Non-stationarity

1 Introduction

Proxy records for the last 11 000 years have documented disruptions in Holocene climate on regional to global scales (e.g., Fairbridge and Hillaire-Marcel, 1977; Barber et al., 2004; Kim et al., 2007). Disruptions are generally perceived as shifts in a record that exceed a predefined level of noise. These shifts in climatological variables also deviate from long-term regional base line trends which are evident from the data reviews of, e.g., Mayewski et al. (2004), Rimbu et al. (2004), or Wanner et al. (2008).

Prominent examples for Holocene climate shifts are the Saharan desertification at around 5.5 kyr BP (thousand years before present) (e.g., Claussen et al., 1999) and the 8.2 kyr BP event (e.g., Renssen et al., 2001). Both shifts have been reproduced by numerical modeling. In this respect they are exceptional because model based understanding of processes underlying regional climate disruptions is still limited.

Apart from the singular 8.2 and 5.5 kyr BP events, many climate shifts appear to be recurrent. Empirical evidence for nearly regular cyclicity in climatolgical variables is accumulating since long: Predominant modes on millennial time scales had been identified by Fairbridge and Hillaire-Marcel already in 1977. The quasi 1450 yr periodicity documented for the North Atlantic by Bond et al. (1997) was referred to in many Holocene climate studies, even for tropical regions (deMenocal et al., 2000; Thompson et al., 2003). Recurrent climate anomalies were also detected on centennial or decadal time scales (McDermott et al., 2001; Benson et al., 2002; Sarnthein et al., 2003).

Oscillatory behavior may be connected to oceanic overturning over a wide range of periodicities (Sevellec et al., 2006; Weijer and Dijkstra, 2003). Oscillations and their trigger mechanisms are, however, poorly understood. Uncertainty in forcing factors and the complexity in the (regional) interplay between atmosphere, ocean, ice, and vegetation are both substantial (Steig, 1999). Solar activity was proposed as an important external trigger (e.g., van Geel et al., 2000; Hodell et al., 2001b; Bond et al., 2001; Gupta et al., 2005). Alternatively, insolation variations at low frequency may have modulated high frequency modes and related teleconnections (Clement et al., 1999; Lohmann and Lorenz, 2007).

Relevant driving mechanisms such as the forcing of modes, or coupling between subsystems can potentially be identified using spectral methods. Analyses in the frequency domain can disclose system properties of the regional or global climate (like regularity of modes) and, when extended to external forcings, may also point to the possible origin of shifts (Gupta et al., 2005; Debret et al., 2007). A spectral analysis of a set of distinct high-resolution records in particular helps to understand interconnections in the climate system.

For regional systems like the South Pacific (Moy et al., 2002) or North Atlantic

(Debret et al., 2007), spectral analysis indicated non-stationarity in Holocene climate variability. Detected discontinuities tend to accumulate around 5-6 kyr BP what would . Intermittency of the climate system, apparent in the lack of mode continuity, is, however, found throughout the Holocene, particularly in the last 6000 years (Moberg et al., 2005; Wanner et al., 2008). It thus remains unclear whether non-stationarity in variability modes is a common feature of regional climate systems, and, more specifically, whether it is more likely to occur during the mid-Holocene (cf. Wanner et al., 2008). For approving a mid-Holocene temporal reorganization of fluctuation modes an analysis covering the entire Holocene period is required.

Another relevant aspect of Holocene climate variability is its spatial organization. A refined knowledge about spatial correlations in oscillatory modes can be expected to improve modeling, but also interpretation of shifts observed in local proxy records. Some studies have provided estimates for the lateral range of prominent disruptions or fluctuations (deMenocal et al., 2000; Sirocko, 2003; Mayewski et al., 2004; Seppä et al., 2007). Consistent regional differences of millenial climate variability were shown for the tropics and high latitudes (Rimbu et al., 2004) based on alkenone sea surface temperature (SST) proxy records. Also the review works of Morrill et al. (2003), Moberg et al. (2005), or Wanner et al. (2008) delineate regional structures in variability modes.

Synthesis studies containing both spatially explicit and spectrally resolved information, however, are built on a small number of records. In addition to the limited number of existing records, focus on a single climatological variable (like SST or air temperature), a specific region (e.g. by Debret et al., 2007), or on a shorter interval within the Holocene (e.g. by Moberg et al., 2005) further downsizes coverage. Still incomplete data availability hinders a statistically robust characterization of non-stationarity or spatial correlation.

We therefore propose a spectral analysis that relies on a broad selection of proxy time series with a quasi-global coverage and for the entire Holocene. We assume that variability in single but relevant climatological variables often indicate the presence or absence of fluctuation modes also of other parts of the climate system (Petit et al., 1999), and that variations in one variable like SST might well have influenced another variable (e.g. air temperature) in spatial proximity. For example, various proxies (δ^{18}O, grayscale density, dust concentration) from sites adjacent to the Peruvian upwelling area show significantly stronger fluctuations after the mid-Holocene (Rosenthal et al., 2003; Rodbell et al., 1999; Moy et al., 2002; Thompson et al., 2003). Both, reconstructed temperature for Central Europe (Davis et al., 2003) and pollen inferred precipitation for the Swiss Alps (Wick et al., 2003b) reveal the opposite trend of stronger variability in the Lower compared to the Upper Holocene.

Although the records collected in this study reflect different aspects of locally specific climates, the variables are neither totally disparate (i.e. here restricted to few categories), nor do they systematically differ with respect to their propensity to show disruptions or fluctuations. Performing, in addition, analyses in the frequency domain, we deliberately exclude detection of trends or of the relative phase of modes (synchronicity). With the mere focus on (dis)appearance of non-stationary modes, our power spectrum technique resolves variability changes in a highly aggregated way. The wide spatio-temporal domain allows to use a large number of published records. This should enable a statistically robust synthesis of spectral results, even concerning their change over the Holocene or across different regions. Our analysis can stimulate and guide more mechanistic approaches, like separated analysis of single variables, or modelling.

We address the following three questions: (1) How are variability modes of Holocene climate distributed around the globe? (2) Does the majority of them reveal non-stationarity at mid-Holocene? (3) If yes, are those mid-Holocene alterations in climate variability spatially correlated?

Alike other studies on spectral characteristics, this work has to disentangle singular events (like the 8.2 and 5.5 kyr BP events mentioned above) from recurrent disruptions. Furthermore, and like other review studies, it has to carefully consider the different quality of records, in particular in terms of time resolution and dating uncertainties. Thus, information on age model errors is to be assembled, and synthesized to a representative error statistics. Extensive sensitivity tests will then quantify how either the definition (or account) of singular events, and age model uncertainties affect our results. In doing so, we not only check for reliability, but also propose a methodological repertoire for an integrated (spectral) analysis of multiple proxy records.

2 Materials and methods

2.1 Selection of proxy data

We chose a range of proxies that represent major climatological variables such as temperature, precipitation, and wind regime. Our selection did not include records that involve more complex or possibly lagged relationships to climate, such as productivity, lake level, glacier advances or stable carbon isotopes. The types of proxy variables are categorized in Tab. 1 into (1) isotope fractionation, mostly $\delta^{18}O$, (2) lithic composition, and (3) relative species abundance (tree pollen or algae). In addition, solar activity was inferred from ^{10}Be abundance and ^{14}C flux (Bond et al., 2001).

Due to low sedimentation rate resulting in coarse temporal resolution, open ocean locations are underrepresented with respect to terrestrial and coastal sites (Fig. 1).

In total we collected 124 long-term high-resolution time series obtained at 103 globally distributed sites from existing literature. 79% of the records have temporal resolution better than 100 yr (more than 90% have average spacing below 180 yr) and 82% span more than 9 000 yr within the period 11 kyr BP to the present (see Tab. 1 and Tab. 2). 68 data sets are accessible from the Publishing Network for Geoscientific & Environmental Data (PANGEA, www.pangea.de) or the National Climate Data Center (NOAA NCDC, www.ncdc.noaa.gov). The remaining time series were digitized with an error of less than 2% from original publications (estimated using 2 digitally available records).

2.2 Lomb-Scargle spectral analysis

Non-stationarity in geoscientific time-series has repeatedly been treated with wavelet analysis (Moy et al., 2002; Moberg et al., 2005; Debret et al., 2007). However, wavelet transformations in general require evenly sampled time-series, while time sequences of proxy records are mostly irregular. Only Witt and Schumann (2005) tested (technical) applicability to unevenly spaced data in a single, rather time-homogeneous case. Wavelet analysis, in addition, produces a high amount of output which is difficult to translate into first order variability trends without additional assumptions. Output of wavelet analysis, finally, has to be carefully interpreted, especially in terms of statistical significance (Maraun and Kurths, 2004).

We therefore base our analysis on an extended version of the Lomb-Scargle approach suggested by Schulz and Mudelsee (2002). The method has been robustly applied to a high number of (unevenly spaced) time-series. After employing a Lomb-Scargle Fourier transform followed by a bias correction with correction factor obtained from a theoretical red-noise spectrum, modes can be tested for significance (Sarnthein et al., 2003; Gupta et al., 2005; Wanner et al., 2008). Here, we employ version 3.5 of the software package REDFIT (Schulz and Mudelsee (2002), www.ncdc.noaa.gov/paleo/softlib/redfit/redfit.html), using two Welch windows (50% overlap) and oversampling factor 4, and assume a 95% confidence level for identifying significant spectral anomalies. For time series with a small fraction (n) of data points in each Welch window, we follow the recommendation by Thomson (1990) and take $1 - 1/n$ as the threshold for significance.

2.3 Window bootstrapping

To detect non-stationarity in spectral behavior we combine the REDFIT algorithm with a bootstrapping approach. We employ bootstrapping in two consecutive steps, the first of which for seeking the time period with minimal spectral coherence. In this step, all data outside a window of 4 kyr length are bootstrapped, similar to the technique described by Zhang et al. (2005). Randomly chosen data points are substituted with also randomly chosen values from the same time-series (outside the window). Results reliably converge when using 5 000 realizations with substitution fraction of 33% for each time series. Subsequently, we examine the spectrum for significant modes by the Lomb-Scargle analysis prior and after bootstrapping. By moving the window from the start of the time-series to its end, and comparing with the number of significant periods before selective bootstrapping, we quantify the localized contribution to the original power spectrum.

As shown in Fig. 2, the window in average contains a high fraction of periodic modes compared to the surrounding interval, when located in the Upper or the Lower Holocene part of all records. This ratio decays down to a quarter of its maximum value at 5.5 kyr BP (center point of the non-bootstrapped 4 kyr window), indicating a global discontinuity of modes in this period.

Given the spectral discontinuity around 5.5 kyr BP and acknowledging the existing notion of a mid-Holocene climatic change (e.g. Steig, 1999; Morrill et al., 2003) we divide the time series into two overlapping intervals; these intervals (11–5 kyr BP and 6–0 kyr BP) will be referred to as Lower and Upper Holocene, respectively. The initial age 11 kyr BP compromises between the different starting points of the time-series, which in some cases reflect the globally asynchronous onset of the Holocene. Neither the choice of the starting age nor of the split point is found to be critical for our analysis, mainly due to the high number of considered time-series (see below).

Based on this bisection, a second bootstrap discloses local long-term switches in the variability signal. As for the moving window analysis described above, data outside the Lower or Upper Holocene are randomly replaced and the time-series subsequently analyzed using the REDFIT algorithm. Differences in spectral significance with respect to the original time-series indicate sensitivity to bootstrapping and, thus, non-stationarity of modes. If a mode looses significance by bootstrapping in the upper interval, but endures changes in the lower part, this corresponds to a positive change in cyclicity (periodic signal originates from the Upper Holocene part of the time-series). The opposite behavior (sensitivity in bootstrapping the lower and robustness in the upper time interval) defines a temporal decrease in variability.

2.4 Sensitivity tests

Singular (geomorphological) events in the Holocene differ from inherent oscillations of the climate system. One example is the catastrophic freshwater drainage from Lake Agassiz around 8.2 kyr BP and its likely effect on ocean circulation (Clarke et al., 2003; Kleiven et al., 2008). To test relevance of such singularities, we repeat the entire analysis after treating the time-series at the Younger Dryas to postboreal transition and around the 8.2 kyr event: When anomaly intensity exceeds unity in the periods 8–8.4 (as is the case in only 18% of records) and 10.6–11 kyr BP, all data in the respective interval are rescaled so that anomaly intensity of the detrended time-series falls below unity (cf. lower left plot in Fig. 3).

As a second sensitivity test, we check for effects of possible dating uncertainties. To this end, we reviewed the published age models, finding that >80% of available chronostratigraphies had 6–14 dated samples and dating uncertainty (σ) between 20 and 120 yr, generally increasing with age and decreasing with the number of datings. Exceptions are, for example, ice cores with much higher precision. The variety of techniques (C^{14}, Th^{230}/U^{234}, varve chronology) motivated a ubiquitous treatment of the entire set of time series. Emulating the maximal distortion compatible with the average uncertainty statistics, all records were divided into 8 sections which were alternatingly stretched and condensed by σ=120 yr (cf. upper left plot in Fig. 3). Sectional iteration of dilation/compression will produce an upper estimate of the possible distorting effect, i.e. enlarge the spacing of two sample points by up to 240 yr, so that uncertainties are largely overestimated in particular for Upper Holocene strata. Spectral analysis on distorted time-series is performed as described above for the untreated time series.

2.5 Geospatial analysis and clustering

To obtain spatial information, we apply spatial autocorrelation analysis (Moran's I, Legendre and Legendre (1998)) on outcomes of the extended Lomb-Scargle analysis (i.e. spectral significance changes). As standard weights of the link between two sites we use the inverse of the distance (with an offset of 100 km if records originated from the same or an adjacent location). Distances are binned such that each bin size equals 400 pairs. Moran's I is then computed for each bin. We test significance of the resulting correlogram after Bonferroni correction of the significance level α. The correction accounts for the inter-dependency of data in different bins in a conservative way (Oden, 1984; Legendre and Legendre, 1998). We also searched for zonal effects by treating longitudinal and latitudinal distances separately.

Significance of the spatial correlogram together with a change in the sign of I (at distance $2R$) indicate a strong patchiness in spectral behavior. The typical autocorrelation length of $2R$ can be translated into a geographical visualization by extrapolation. From each proxy location, spectral intensity

S' of the record (or its change) radially spreads in all directions, whereby S' exponentially decreases with distance r ($S'(r) = S \cdot \exp(-r/R)$ with half influence distance R). Peak intensity is a binary measure with $S = 1$ in the case of presence/increase of frequencies, and $S = -1$ for absence or negative trends. Colored contour maps visualize the sum $\sum S'$ at each point on a 1° resolution grid.

2.6 Non-cyclic event frequency

Outcomes of the spectral analysis are cross-checked by a simple counting method relying on a straightforward definition of climate events. After removal of the 2 kyr running mean, we normalize the time series by their standard deviation. We then consider frequency peaks as a distinct event if (1) they exceed a threshold p_a and (2) are separated by a zero-line crossing to the preceding event. By using in parallel a set of thresholds $p_a = 1.5^{-1,0,1,2}$ we remove most sensitivity with respect to a specific choice of p_a. The non-cyclic event frequency is calculated as the average number of events for all thresholds p_a, divided by the length of the time period.

3 Results

3.1 Mid-Holocene change

Discontinuity of modes during the mid-Holocene is evident from the loss in significant modes in a moving window with respect to modes detected outside the window (Fig. 2). The total number of modes inside divided by the number outside the window continously declines towards a minimum at mid-Holocene: there is a spectral feature common to most of the 124 proxy records despite their different relations to the climate state. This not only motivates the specific choice of splitting all timeseries at 5.5 kyr BP for the subsequent analysis but may also indicate a structural change in global climate in this period (cf. Wanner et al., 2008).

Fig. 3 visualizes the way how mid-Holocene changes in the spectral intensity are detected by our method. Representative for different spectral changes are two selected records, i.e. δ^{18}O variations in Soreq Cave, Israel (lower panels), and δ^{18}O at Sajama, Bolivia (upper panels). Only those frequency peaks that are with 95% probability not compatible with red noise mark a significant mode (center panels in Fig. 3 and dashed-dotted lines therein). Random displacement of proxy values in one half of the Holocene dampens some of those modes, as, for example, obvious for the two centennial cycles (415 and 280 yr) in the Soreq record during the Upper Holocene. For δ^{18}O at Sajama, spectral changes are manifold. The 860 yr mode vanishes when either of the two halves is randomized by bootstrapping, and the two prominent centennial cycles (250 yr, 200 yr) re-appear in the Upper Holocene while missing in the preceding interval.

Apart from the two example records, we detect in all 124 time series 188 significant modes in the spectral range between 1/200 yr^{-1} and 1/1800 yr^{-1}. These are distributed over 97 records, 27 time-series do not contain a dominant period. When contrasting Lower with Upper Holocene, only 68 of these peaks occur before 5.5 kyr BP while 87 modes gain or persist significance thereafter. Sensitivity of most records to a sectional bootstrap indicates non-stationarity of climate oscillations. Only about 10% of spectral peaks are stable, i.e. found before and after partial bootstrapping.

3.2 Regional clustering of spectral properties

Only a minority of sites document significant modes in the Lower Holocene as obvious from the mapping of oscillations on a global scale (Fig. 4). These sites are mainly grouped into a North Atlantic domain, both polar regions, and into a narrow band in central Asia (red areas in lower panel of Fig. 4). In the Upper Holocene (upper panel in Fig. 4), the western Atlantic and the majority of East American sites form large regional clusters characterized by strong periodic variability. Like for the Lower Holocene, East Asian records do not offer uniform evidence of dominant modes, with the tendency that no significant peaks appear in Lomb–Scargle periodograms. In most other world regions, between 180° W and approximately 75° E, presence and absence of modes turn out to be clustered in a complementary way when contrasting Upper and Lower Holocene. As a consequence, changes in variability from the Lower to the Upper Holocene are even more uniformly organized in space (Fig. 5).

The patches or bands are not zonally distributed, but geographically. In part, this is due to the concentration of proxy sites near coasts. Orientation of clusters along continental coastlines most strikingly appears in the two Americas, to some extent also in Africa and Europe. Zonal independence is, in addition, confirmed by the autocorrelation analysis using longitudinal or latitudinal distances (not shown).

Uniform clusters in Fig. 5 typically consist of six to ten proxy records with identical spectral trend. Modes consistently appeared during the Mid-Holocene in North-East and South-East America, central and eastern Europe, Africa (western and southern part), while periodic variability declined around the North Atlantic, central to eastern Asia and along western South America. Damping or amplification of climate fluctuations is robustly attributed to sub-continental scale regions.

The spatial organization of clusters is only moderately affected by mapping the change for two frequency bands in Fig. 6. Since the total bandwidth is higher for all centennial modes (1/200 yr – 1/850 yr), their global trend pattern largely resembles the one for the entire frequency band (1/200 yr – 1/1800 yr). In contrast, millennial cycles are geographically less concentrated, apart from some weak grouping of dampened 850–1 800 yr cycles around the North Atlantic basin. Within the fraction of only 27% records containing millennial modes we observe only few persistent cycles, more modes arising during mid-Holocene, and mostly modes that cease at that time.

Coherence of mode (in)activation within regional clusters is supported by spatial for the visual extrapolation has been set to $R = 1\ 500\,\mathrm{km}$ in all maps (Figs. 4-6, 8).

4 Discussion

4.1 Robustness of results and cross-validation

4.1.1 Global coverage

Spatial uniformity in variability trend at a sub-continental scale consistently appeared despite the heterogeneous type and quality of records, inherent random noise or other local phenomena. For detecting consistent regional signatures the number of records turns out to be sufficient, also because of the coarse temporal differentiation between Upper and Lower Holocene (as highly aggregated measure for non-stationarity). The discriminative power arising from signal aggregation and global coverage of sites is most obvious from the high statistical significance level which can be attributed to the (negative) spatial autocorrelation at distance of about 4 500 km.

So far, non-stationary variability has only been reported for regional systems like the Southern Pacific with its decadal to centennial cyclicity related to the El Niño Southern Oscillation (ENSO) by Moy et al. (2002). Previous review studies, however, were not emphasizing the global dimension of the reorganization between Lower and Upper Holocene. One reason for this may be the reference character of Greenland and the North Atlantic. Records from this area show persistent millennial cycles (Bond et al., 1997), in contrast to nearly all other locations around the globe at which modes are generally non-stationary.

4.1.2 *Dating uncertainties and singular events*

The unexpected coherency may also follow from other methodological features like much reduced sensitivity of spectral results to potential dating errors. Standard approaches like temporal correlation between spatially distributed proxy time-series, in contrast, critically depends on age model accuracy. Some sensitivity to dating also appears in our study. Already in the example periodogram for δ^{18}O in the central Andes (Sajama, Fig. 3), characteristic frequencies and spectral intensities are modified after a severe distortion of the underlying chronology. Instead of 3 dominant modes, the spectrum of the distorted time-series then contains 4 (significant) peaks. The indication for increased climate variability in the Andes region (from the Lower to the Upper Holocene), however, turns out to be robust as no mode is detected for the Lower Holocene and still a 210 yr cycle pervades to the Upper Holocene after time-series manipulation. This individual finding can be generalized to the entire collection of records because only in 10.5% of cases, time distortion affects Upper/Lower Holocene switches in significant spectral peaks. Also the regional patterning of mode changes turned out to be close to the undisturbed analysis (map not shown due to resemblance to Fig. 5). Hence, differences in the quality of age models have only a limited effect on our spectral synthesis.

The removal of singular events that represent geomorphological singularities like the 8.2 kyr BP event exerts a similarly small influence on the periodogram (cf. Soreq cave δ^{18}O record, Fig. 3), as about 15% of all records changed their variability trend upon removal of singularities.

Taken together, an aggregated spectral view reduces (not deletes) sensitivity to specific methodological settings or to inherent errors such as inaccurate chronologies. The binary nature of output information facilitates an up-scaling to the global scale where possible artifacts of individual records tend to average out due to the high number of analyzed time-series.

4.1.3 Non-cyclic event density

Our spectral method is in line with density changes in non-cyclic anomalies from the first to the second half of the Holocene. Non-cyclic variability trends turn out to be spatially coherent within bands and regions which are globally organized similar to periodic variability (Fig. 8). The North Atlantic basin scale decline in climate variability, however, is in this picture shifted to the West, now including Europe but not North America. There, trends in the eastern and western part have swapped their sign with respect to trends in periodic modes (cf. Fig. 5).

Abundance of climatic anomalies increases in many East Asian sites where one would expect a decrease according to the spectral analysis. There is considerable scatter in anomaly-based variability trends within the East Asian monsoon system. The scattering and partial inconsistency with the periodic picture may be due to the internal complexity of the monsoon and various active teleconnections to which it is sensitive. For example, it has been speculated that the atmospheric connection between the western Asian monsoon and the large-scale thermohaline circulation in the North Atlantic decreased in intensity from the Lower to the Upper Holocene (Morrill et al., 2003). While the teleconnection might explain the similarity in spectral shifts, its reduction may be responsible for a low correlation between trends in non-cyclic variability in the two climate subsystems. In general, clusters with either growing or declining number of climate events appear spatially even more uniform than the regions based on Lomb-Scargle derived trends. Both variability measures agree with respect to a Pan-American corridor and a band from the East African coast across the Arabian Sea to central Asia where climate variability increased during the Holocene.

4.2 Possible mechanisms for variability changes

Understanding of the mechanisms producing quasi-cyclic fluctuations during the Holocene is still fragmented. It could therefore be premature to ask for what has caused their temporal change or their regional organization. We thus only briefly reflect the possible role of ocean and atmospheric circulation, and of external forcings.

4.2.1 Overturning eigenmodes

Though climatic transitions challenge concurrent climate models, it is useful to compare the observed variability with internal oscillatory modes (without external trigger) which are seen in models of reduced complexity (Mikolajewicz and Maier-Reimer, 1990; Weijer and Dijkstra, 2003). Model perturbation experiments reveal eigenmodes on millennial time scales. These modes are generated by the advection of buoyancy anomalies around the overturning loop, both in a single-hemispheric basin leading to centennial modes or throughout the global ocean responsible for millennial cycles (Broecker et al., 1985; Stocker et al., 1992; Weijer and Dijkstra, 2003). The most negative eigenvalues (strongest damping) were found for centennial oscillations (Weijer and Dijkstra, 2003; Te Raa and Dijkstra, 2003). In simulation studies, such modes could be activated if fluctuations in radiative energy input are included (Weber et al., 2004).

4.2.2 Solar influence

The sun's influence on Holocene climate variability has been earlier deduced from the synchronicity of climate anomalies and variations in solar activity (e.g. Bond et al., 2001; Hodell et al., 2001b). Our analysis includes records of cosmogenic nuclide production (^{10}Be and ^{14}C flux) as well as reconstructed sunspot number of Solanki et al. (2004). Two of these three records indicate weakening of the 208 yr Suess cycle, and none contains firm evidence for millennial modes (yellow star in Fig. 5–6). A recent analysis of the sunspot number power spectrum based on a longer part of the time-series and less severe significance criteria identified periods of 6 500, 2 500, 950 and 550 yr, but no 1 500 yr periodicity (Dima and Lohmann, 2009). Debret et al. (2007) already questioned the hypothesis of Bond et al. (2001) that the 1 500 yr cycles are due to variations in solar activity. Still, the possibility of solar variability being amplified by oceanic feedbacks can not be entirely excluded (Renssen et al., 2006).

4.2.3 North Atlantic deep water formation

Central in the literature discussion on Holocene climatic stability is the large-scale ocean circulation and related North Atlantic deep water formation. It is conceivable that ocean circulation changes, like those of the Atlantic multidecadal oscillations, affect variability in the North Atlantic basin on longer time scales. Hydrographic changes linked to ocean circulation variations were more pronounced in the early compared to the late Holocene (Kim et al., 2007). The Iceland–Scotland overflow water is an important component of the ocean circulation. Its record (derived flow velocity) contains dominant periodicities of 1 400 and 700 yr over the Holocene (Bianchi and McCave, 1999; Dima and Lohmann, 2009). Variations are also detected in surface and subsurface hydrographic quantities in the Atlantic Ocean (Rühlemann et al., 2004). It is possible that very strong overturning events around 5 kyr BP (Bianchi and McCave, 1999) could have affected phase-relationships of coupled, weakly oscillating climatic subsystems worldwide.

In contrast to the frequency domain, previous studies looked on spatial patterns in SST trend evolution during the Holocene (Marchal et al., 2002; Lorenz and Lohmann, 2004; Rimbu et al., 2004; Kim et al., 2004; Lorenz et al., 2006). These, for example, identified an in-phase relation of most North Atlantic cores, both for the mid-to-late Holocene trend as well as millennial variability (Rimbu et al., 2004). Part of the variability can be attributed to the Arctic/North Atlantic Oscillation (AO/NAO) as well as the Pacific Decadal Oscillation (PDO), possibly explaining a substantial fraction of spatial clustering which we found in this study. The dominant NAO variability pattern shows slightly enhanced millennial variability in the early Holocene relative to the late Holocene (Rimbu et al., 2004). However, in this kind of pattern analysis (using EOF), variability in individual records is partially filtered out, and for a rigorous analysis of high-frequency variability (less than 1 000 yr), the available marine data are too sparse.

4.2.4 Possible origin of global variability changes

The mechanisms behind oscillatory state transitions include

Regions with lowered SST notably overlap with those areas that reveal declining variability (cf. Fig. 4, Lorenz et al. (2006) with Fig. 5). The same applies to regions with increased SST. In eastern Europe and Asia, the match becomes even more accurate when referring to regions defined according to changes in non-cyclic event frequency (Fig. 8). The shifts were possibly mediated by dislocations of convergence zones or trade winds, thereby modifying the damping and amplification forces of modes (Dima and Lohmann, 2004; Lohmann and Lorenz, 2007). Indeed, Fig. 4 shows enhanced variability for the Upper Holocene in the upwelling regions (in addition to continental Europe), in contrast to enhanced variability in the northern North Atlantic for the Lower Holocene.

As a result of low frequency control, oceanic or atmospheric teleconnections between subsystems could have weakened or strengthened.

It has been found that the PDO and the El Niño-Southern Oscillation (ENSO) show punctuated enhancement at mid-Holocene (Moy et al., 2002). The origin of high frequency fluctuations is controversially discussed but a combination of nonlinear interactions in the tropical Pacific and orbital forcing is likely to activate these modes (Clement et al., 1999; Loubere et al., 2003; Simmonds and Walland, 1998).

5 Conclusion

Our results support the hypothesis that around 5-6 kyr BP the climate system has undergone a reorganization in variability. The statistical analysis is based on a description of fluctuation changes that transforms non-stationarity into binary Lower to Upper Holocene transitions, thereby revealing a notable uniformity within large-scale clusters.

Coverage of proxy records has to be raised in many regions, especially throughout the global ocean, in order to further substantiate the regional character of mid-Holocene changes. Still, the density of records used in this study already creates sufficient robustness with respect to possible errors connected to individual time-series. Regional differences in fluctuation changes are persistently detected using different methodologies (spectral and non-periodic analysis), or taking into account dating uncertainties and the effect of singularities.

In short, our findings translate to a simple rule: given a Holocene record that shows a change in variability, other records of possibly different type, but in geographical proximity will probably exhibit the same change. Hence, our initial assumption on a spatial and/or causal relation between fluctuation modes in different climatological variables leads to a description of Holocene climate variability which allows for mechanistic interpretation. An increase in North Atlantic variability in the early part of the Holocene could be possibly linked to reorganizations of the ocean circulation due to the shift from cold to warm conditions and the complete loss of the North American ice sheets. The enhanced variability for the late Holocene in the upwelling regions off the coasts of Africa and America could be related to increased thermal gradients between high and low latitudes caused by the insolation forcing (Lorenz and Lohmann, 2004; Rimbu et al., 2004; Lorenz et al., 2006). The mid-Holocene is in particular coined by the termination of the African Humid Period. We hypothesize that the disruptive effect of this event and/or adiabatic external control slightly modified coupling intensity between subsystems (regional interplay of atmosphere, ocean, ice, and vegetation), turning these subsystems either more or less prone to oscillations. An integrated understanding of mechanisms behind non-stationarity and regional structuring in Holocene climate thus defines a reasonable challenge for modelling studies.

6 Acknowledgements

We thank the data contributors. We are grateful to Victor Brovkin, , and one anonymous reviewer for helpful comments. Sabrina Solms and Sonja Dorendorf are acknowledged for assisting with the compilation of data and literature. C.L was supported by the Deutsche Forschungsgemeinschaft (DFG priority program 1266 INTERDYNAMIK) and the Dutch Agency for Environmental Assessment (MNP Bilthoven). K.W and G.L. were supported by the Helmholtz society via the programme PACES.

References

Andreev, A., Tarasov, P., Siegert, C., Ebel, T., Klimanov, V., Melles, M., Hahne, J., Shilova, G., Dereviagin, A., Hubberten, H.-W., 2003. Vegetation and climate changes on the northern Taymyr, Russia during the upper Pleistocene and Holocene reconstructed from pollen records. Boreas 32, 484–505.

Arz, H. W., Gerhardt, S., Pätzold, J., Röhl, U., 2001. Millennial-scale changes of surface- and deep-water flow in the western tropical Atlantic linked to northern hemisphere high-latitude climate during the Holocene. Geology 29, 239–242.

Bar-Matthews, M., Ayalon, A., Kaufman, A., Wasserburg, G. J., 1999. The Eastern Mediterranean paleoclimate as a reflection of regional events: Soreq cave, Israel. Earth Planet. Sci. Lett. 166, 85–95.

Barber, D., Dyke, A., Hillaire-Marcel, C., Jennings, A., Andrews, J., et al., 1999. Forcing of the cold event of 8,200 years ago by catastrophic drainage of Laurentide lakes. Nature 400, 344.

Barber, K., Zolitschka, B., Tarasov, P., Lotter, A. F., 2004. Atlantic to Urals – the Holocene climatic record of mid-latitude Europe. In: R.W. Battarbee, F. G., Stickley, C. (Eds.), Past Climate Variability through Europe and Africa. Vol. 6 of Developments in Paleoenvironmental Research. Springer, Dordrecht, pp. 417–442.

Barker, P. A., Street-Perrott, F. A., Leng, M. J., Greenwood, P. B., Swain, D. L., Perrott, R. A., Telford, R. J., Ficken, K. J., 2001. A 14,000-year oxygen isotope record from diatom silica in two alpine lakes on Mt. Kenya. Science 292, 2307–2310.

Benson, L., Kashgarian, M., Rye, R., Lund, S., Paillet, F., Smoot, J., Kester, C., Mensing, S., Meko, D., Lindström, S., 2002. Holocene multidecadal and multicentennial droughts affecting northern California and Nevada. Quat. Sci. Rev. 21, 659–682.

Bianchi, G., McCave, I., 1999. Holocene periodicity in North Atlantic climate and deep-ocean flow south of Iceland. Nature 397, 515–517.

Bond, G., Kromer, B., Beer, J., Muscheler, R., Evans, M. N., Showers, W., Hoffmann, S., Lotti-Bond, R., Hajdas, I., Bonani, G., 2001. Persistent solar influence on North Atlantic climate during the Holocene. Science 294, 2130–2136.

Bond, G., Showers, W., Cheseby, M., Lotti, R., Almasi, P., deMenocal, P., Priore, P., Cullen, H., Hajdas, I., Bonani, G., 1997. A pervasive millennial-scale cycle in North Atlantic Holocene and glacial climates. Science 278, 1257–1266.

Bonnefille, R., Chalie, F., 2000. Pollen-inferred precipitation time-series from equatorial mountains, Africa, the last 40 kyr BP. Global Planet. Change 26, 25–50.

Brachfeld, S., Acton, G. D., Guyodo, Y., Banerjee, S. K., 2000. High-resolution paleomagnetic records from Holocene sediments from the Palmer Deep, Western Antartic Peninsula. Earth Planet. Sci. Lett. 181, 429–441.

Broecker, W., Peteet, D., Rind, D., 1985. Does the ocean-atmosphere system have more than one stable mode of operation? Nature 315, 21–25.

Camill, P., Umbanhowar, C. E., Teed, R., Geiss, C. E., Aldinger, J., et al., 2003. Late-glacial and Holocene climatic effects on fire and vegetation dynamics at the prairie forest ecotone in south-central Minnesota. J. Ecol. 91, 822–836.

Carcaillet, C., Bergeron, Y., Richard, P., Fréchette, B., Gauthier, S., Prairie, Y., 2001. Change of fire frequency in the eastern Canadian boreal forests during the Holocene: does vegetation composition or climate trigger the fire regime? J. Ecol. 89, 930–946.

Chapman, M. R., , Shackleton, N. J., 2000. Evidence of 550-year and 1000-year cyclicities in North Atlantic circulation patterns during the Holocene. Holocene 10, 287–291.

Clarke, G., Leverington, D., Teller, J., Dyke, A., 2003. Superlakes, Megafloods, and Abrupt Climate Change. Science 301, 922–923.

Claussen, M., Kubatzki, C., Brovkin, V., Ganopolski, A., Hoelzmann, P., Pachur, H., 1999. Simulation of an abrupt change in Saharan vegetation at the end of the mid-Holocene. Geophys. Res. Lett. 24, 2037–2040.

Clement, A., Seager, R., Cane, M., 1999. Orbital controls on the El Niño Southern Oscillation and the tropical climate. Palaeoceanogr. 14, 441–456.

Cruz, F., Burns, S., Karmann, I., Sharp, W., Vuille, M., Cardoso, A., Ferrari, J., Dias, P. S., Jr., O. V., Mar. 2005. Insolation-driven changes in atmospheric circulation over the past 116, 000 years in subtropical Brazil. Nature 434, 63–66.

Curtis, J., Brenner, M., Hodell, D., 1999. Climate change in the Lake Valencia Basin, Venezuela, $\approx 12600\,\mathrm{yr\,BP}$ to present. Holocene 9, 609–619.

Curtis, J. H., Brenner, M., Hodell, D. A., Balser, R. A., Islebe, G. A., Hooghiemstra, H., 1998. A multi-proxy study of Holocene environmental change in lowlands of Peten, Guatemala. J. Paleolimnol. 19, 139–159.

Curtis, J. H., Hodell, D. A., Brenner, M., 1996. Climate variability on the yucatan peninsula (mexico) during the past 3500 years, and implications for maya cultural evolution. Quat. Res. 46, 37–47.

Davis, B. A. S., Brewer, S., Stevenson, A. C., Guiot, J., Data Contributors, Jul.Aug. 2003. The temperature of Europe during the Holocene reconstructed from pollen data. Quat. Sci. Rev. 22, 1701–1716.

Davis, O. K., 1992. Rapid climate change in coastal southern California inferred from pollen analysis of San Joaquin Marsh. Quat. Res. 37, 89–100.

Debret, M., Bout-Roumazeilles, V., Grousset, F., Desmet, M., McManus, J., Massei, N., Sebag, D., Petit, J., Copard, Y., Trentesaux, A., 2007. The origin of the 1500-year climate cycles in Holocene North-Atlantic records. Clim. Past 3, 569–575.

deMenocal, P., Ortiz, J., Guilderson, T., Sarnthein, M., 2000. Coherent high- and low-latitude climate variability during the Holocene warm period. Science 288, 2198–2202.

Denniston, R., Gonzalez, L., Baker, R.G.and Reagan, M., Asmerom, Y., Edwards, R., Alexander, E., Nov. 1999. Speleothem evidence for Holocene fluctuations of the prairie-forest ecotone, north-central USA. Holocene 9, 671–676.

Dima, M., Lohmann, G., 2004. Fundamental and derived modes of climate variability.application to biennial and interannual timescale. Tellus 56A, 229–249.

Dima, M., Lohmann, G., 2009. Conceptual model for millennial climate variability: a possible combined solar-thermohaline circulation origin for the 1,500-year cycle. Climate Dynamics 32, 301–311.

Doose-Rolinski, H., Rogalla, U., Scheeder, G., Lückge, A., von Rad, U., 2001. High resolution temperature and evaporation changes during the late Holocene in the northeastern Arabian Sea. Palaeoceanogr. 16, 358–367.

Dorale, J., Gonzalez, L., Reagan, M., Pickett, D., Murrell, M., Baker, R., 1992. A high resolution record of Holocene climate change in speleothem calcite from Cold Water Cave, northeast Iowa. Science 258, 1626–1630.

Drysdale, R., Zanchetta, G., Hellstrom, J., Maas, R., Fallick, A., Pickett, M., Cartwright, I., Piccini, L., 2006. Late Holocene drought responsible for the collapse of Old World civilizations is recorded in an Italian cave flowstone. Geology 34, 101–104.

Dykoski, C. A., Edwards, R. L., Cheng, H., Yuan, D., Caic, Y., Zhang, M., Lin, Y., Qing, J., An, Z., Revenaugh, J., 2005. A high-resolution, absolute-dated Holocene and deglacial Asian monsoon record from Dongge Cave, China. Earth Planet. Sci. Lett. 233, 71–86.

Fairbridge, R., Hillaire-Marcel, C., 1977. An 8,000-yr palaeoclimatic record of the "Double-Hale" 45-yr solar cycle. Nature 268, 413–416.

Fengming, C., Tiegang, L., Lihua, Z., Jun, Y., 2008. A Holocene paleotemperature record based on radiolaria from the northern Okinawa Trough (East China Sea). Quat. Int. 183, 115–122.

Finkel, R., Nishiizumi, K., 1997. Beryllium 10 concentrations in the Greenland Ice Sheet Project 2 ice core from 3-40 ka. J. Geophys. Res. 102, 26699–26706.

Fleitmann, D., Burns, S., Mangini, A., Mudelsee, M., Kramers, J., Villa, I., Neff, U., Al-Subbary, A., Buettner, A., Hippler, D., et al., 2007. Holocene ITCZ and Indian monsoon dynamics recorded in stalagmites from Oman and Yemen (Socotra). Quat. Sci. Rev. 26, 170–188.

Fleitmann, D., Burns, S. J., Mudelsee, M., Neff, U., Kramers, J., Mangini, A., Matter, A., 2003. Holocene forcing of the Indian monsoon recorded in a stalagmite from southern Oman. Science 300, 1737–1739.

Fontes, J.-C., Gasse, F., Gibert, E., Feb. 1996. Holocene environmental changes in lake Bangong basin (western Tibet). Part 1: Chronology and stable isotopes of carbonates of a Holocene lacustrine core. Paleogeogr. Palaeoclimatol. Palaeoecol. 120, 25–47.

Freudenthal, T., Meggers, H., Henderiks, J., Kuhlmann, H., Moreno, A., Wefer, G., 2002. Upwelling intensity and filament activity off Morocco during the last 250,000 years. Deep-Sea Res. II 49, 3655–3674.

Gasse, F., 2002. Diatom-inferred salinity and carbonate oxygen isotopes in Holocene waterbodies of the western Sahara and Sahel (Africa). Quat. Sci. Rev. 21, 737–767.

Grootes, P., Stuiver, M., 1997. Oxygen 18/16 variability in Greenland snow and ice with 10^{-3}- to 10^{5}-year time resolution. J. Geophys. Res. 102, 26455–26470.

Grootes, P. M., Steig, E. J., Stuiver, M., Waddington, E. D., Morse, D. L., 1994. A new ice core record from Taylor Dome, Antarctica. Eos 75, 225.

Gupta, A., Anderson, D., Overpeck, J., 2003. Abrupt changes in the Asian southwest monsoon during the Holocene and their links to the North Atlantic ocean. Nature 421, 354–356.

Gupta, A., Das, M., Anderson, D., 2005. Solar influence on the Indian summer monsoon during the Holocene. Geophys. Res. Let. 32, L17703.

Haug, G. H., Hughen, K. A., Sigman, D. M., Peterson, L. C., Röhl, U., 2001. Southward migration of the intertropical convergence zone through the Holocene. Science 293, 1304–1308.

Herzschuh, U., Tarasov, P., Wünnemann, B., Hartmann, K., 2004. Holocene vegetation and climate of the Alashan Plateau, NW China, reconstructed from pollen data. Paleogeogr. Palaeoclimatol. Palaeoecol. 211, 1–17.

Higuera-Gundy, A., Brenner, M., Hodell, D. A., Curtis, J. H., Leyden, B. W., Binford, M. W., 1999. A $10,300\,^{14}\mathrm{C}\,\mathrm{yr}$ record of climate and vegetation change from Haiti. Quat. Res. 52, 159–170.

Hodell, D., Curtis, J. H., Brenner, M., 1995. Possible role of climate in the collapse of the Classic Maya civilization. Nature 375, 391–394.

Hodell, D., Kanfoush, S., Shemesh, A., Crosta, X., Charles, C., Guilderson, T., 2001a. Abrupt cooling of Antarctic surface waters and sea ice expansion in the South Atlantic sector of the Southern Ocean at 5000 cal yr B.P. Quat.

Res. 56, 191–198.

Hodell, D. A., Brenner, M., Curtis, J. H., Guilderson, T., 2001b. Solar forcing of drought frequency in the Maya lowlands. Science 292, 1367–1370.

Holmgren, K., Lee-Thorp, J., Cooper, G., Lundblad, K., Partridge, T., Scott, L., Sithaldeen, R., Talma, A., Tyson, P., 2003. Persistent millennial-scale climatic variability over the past 25 thousand years in southern Africa. Quat. Sci. Rev. 22, 2311–2326.

Hu, F. S., Ito, E., Brubaker, L. B., Anderson, P. M., 1998. Ostracode geochemical record of Holocene climatic change and implications for vegetational response in the northwestern Alaska range. Quat. Res. 49, 86–95.

Huang, C.-Y., Liew, P.-M., Zhao, M., Chang, T.-C., Kuo, C.-M., Chen, M.-T., Wang, C.-H., Zheng, L.-F., 1997. Deep sea and lake records of the southeast Asian paleomonsoons for the last 25 thousand years. Earth Planet. Sci. Lett. 146, 59–72.

Hughes, M. K., Graumlich, L. J., 1996. Climatic variations and forcing mechanisms of the last 2000 years. multi-millenial dendroclimatic studies from the western United States. NATO ASI Series 141, 109–124.

Husum, K., Hald, M., 2004. A continuous marine record 8000–1600 cal. yr BP from the Malangenfjord, north Norway: foraminiferal and isotopic evidence. The Holocene 14, 877–887.

Jin, Z., Wu, J., Cao, J., Wang, S., Shen, J., Gao, N., Zou, C., 2004. Holocene chemical weathering and climatic oscillations in north China: evidence from lacustrine sediments. Boreas 33, 260–266.

Johnson, T. C., Brown, E. T., McManus, J., Barry, S., Barker, P., Gasse, F., 2002. A high-resolution paleoclimate record spanning the past 25, 000 years in southern East Africa. Science 296, 113–132.

Jones, V. J., Leng, M. J., Solovieva, N., Sloaneb, H. J., Tarasovc, P., 2004.

Holocene climate of the Kola Peninsula; evidence from the oxygen isotope record of diatom silica. Quat. Sci. Rev. 23, 833–839.

Jung, S., Davies, G., Ganssen, G., Kroon, D., 2004. Synchronous Holocene sea surface temperature and rainfall variations in the Asian monsoon system. Quat. Sci. Rev. 23, 2207–2218.

Keigwin, L. D., 1996. The little Ice Age and medieval warm period in the Sargasso Sea. Science 274, 1503–1508.

Kienast, M., Steinke, S., Stattegger, K., Calvert, S. E., 2001. Synchronous tropical South China Sea SST change and Greenland warming during deglaciation. Science 291, 2132–2134.

Kim, J., Meggers, H., Rimbu, N., Lohmann, G., Freudenthal, T., Müller, P., Schneider, R., 2007. Impacts of the North Atlantic gyre circulation on holocene climate off northwest Africa. Geology 35, 387–390.

Kim, J., Rimbu, N., Lorenz, S., Lohmann, G., Nam, S., Schouten, S., Ruehlemann, C., Schneider, R., 2004. North Pacific and North Atlantic sea-surface temperature variability during the Holocene. Quat. Sci. Rev. 23, 2141–2154.

Kim, J.-H., Schneider, R. R., 2003. Low-latitude control of interhemispheric sea-surface temperature contrast in the tropical Atlantic over the past 21 kyears: the possible role of SE trade winds. Clim. Dyn. 21, 337–347.

Kleiven, H., Kissel, C., Laj, C., Ninnemann, U., Richter, T., Cortijo, E., 2008. Reduced North Atlantic deep water coeval with the glacial Lake Agassiz freshwater outburst. Science 319, 60–64.

Knaack, J., 1997. Eine neue Transferfunktion zur Rekonstruktion der Paläoproduktivität aus Gemeinschaften mariner Diatomeen. Berichte Geol. Paläontol. Inst. Univ. Kiel 83, 1–118.

Laird, K. R., Fritz, S. C., Maasch, K. A., Cumming, B. F., 1996. Greater drought intensity and frequency before A.D. 1200 in the northern Great

Plains, USA. Nature 384, 552–554.

Lamy, F., Hebbeln, D., Röhl, U., Wefer, G., Feb. 2001. Holocene rainfall variability in southern Chile: a marine record of latitudinal shifts of the southern westerlies. Earth Planet. Sci. Lett. 185, 369–382.

Lamy, F., Rühlemann, C., Hebbeln, D., Wefer, G., 2002. High- and low-latitude climate control on the position of the southern Peru-Chile Current during the Holocene. Palaeoceanogr. 17, 10.1029/2001PA000727.

Lea, D., Pak, D., Peterson, L., Hughen, K., 2003. Synchroneity of tropical and high-latitude Atlantic temperatures over the last glacial termination. Science 301, 1361–1364.

Legendre, P., Legendre, L., 1998. Numerical Ecology. Elsevier Science.

Liu, J., Houyuan, L., Negendank, J., Mingram, J., Xiangjun, L., Wenyuan, W., Guoqiang, C., 2000. Periodicity of Holocene climatic variations in the Huguangyan Maar Lake. Chinese Sci. Bull. 45, 1712–1718.

Lohmann, G., Lorenz, S. J., 2007. Orbital forcing on atmospheric dynamics during the last interglacial and glacial inception. In: Sirocko, F., Claussen, M., Sanchez-Goni, M. F., Litt, T. (Eds.), The climate of past interglacials. Vol. 7 of Developments in Quaternary Science. Elsevier, pp. 527–546.

Lorenz, S., Kim, J., Rimbu, N., Schneider, R., Lohmann, G., 2006. Orbitally driven insolation forcing on holocene climate trends: Evidence from alkenone data and climate modeling. Paleoceanography 21, doi:10.1029/2005PA001152.

Lorenz, S., Lohmann, G., 2004. Acceleration technique for milankovitch type forcing in a coupled atmosphere-ocean circulation model: method and application for the holocene. Clim. Dyn. 23, 727–743.

Loubere, P., Richaud, M., Liu, Z., Mekik, F., 2003. Oceanic conditions in the eastern equatorial Pacific during the onset of ENSO in the Holocene. Quat.

Res. 60, 142–148.

Maraun, D., Kurths, J., 2004. Cross wavelet analysis: significance testing and pitfalls. Nonlin. Proces. Geophys. 11, 505–514.

Marchal, O., Cacho, I., Stocker, T., Grimalt, J., Calvo, E., Martrat, B., Shackleton, N., Vautravers, M., Cortijo, E., van Kreveld, S., et al., 2002. Apparent long-term cooling of the sea surface in the northeast Atlantic and Mediterranean during the Holocene. Quat. Sci. Rev. 21, 455–483.

Masson, V., Vimeux, F., Jouzel, J., Morgan, V., Delmotte, M., et al., 2000. Holocene climate variability in Antarctica based on 11 ice-core isotopic records. Quat. Res. 54, 348–358.

Mayewski, P., Rohling, E., Stager, J., Karlen, W., Maasch, K., Meeker, L., Meyerson, E., Gasse, F., Holmgren, K., et al., 2004. Holocene climate variability. Quat. Res. 62, 243–255.

McDermott, F., 2004. Palaeo-climate reconstruction from stable isotope variations in speleothems: a review. Quat. Sci. Rev. 23, 901–918.

McDermott, F., Mattey, D., Hawkesworth, C., 2001. Centennial-scale Holocene climate variability revealed by a high-resolution speleothem δ^{18}O record from S.W. Ireland. Science 294, 1328–1331.

Mikolajewicz, U., Maier-Reimer, E., 1990. Internal secular variability in an ocean general circulation model. Clim. Dyn. 4, 145–156.

Moberg, A., Sonechkin, D., Holmgren, K., Datsenko, N., Karlin, W., 2005. Highly variable northern hemisphere temperatures reconstructed from low- and high-resolution proxy data. Nature 433, 613–617.

Morrill, C., Overpeck, J., Cole, J., 2003. A synthesis of abrupt changes in the Asian summer monsoon since the last deglaciation. Holocene 13, 465–476.

Moy, C., Seltzer, G. O., Rodbell, D. T., Anderson, D. M., 2002. Variability of El Niño/Southern Oscillation activity at millennial timescales during the

Holocene epoch. Nature 420, 162–165.

Noren, A., Bierman, P., Steig, E., Lini, A., Southon, J., 2002. Millennial-scale storminess variability in the northeastern United States during the Holocene epoch. Nature 419, 821–824.

Oba, T., Murayama, M., 2004. Sea-surface temperature and salinity changes in the northwest Pacific since the Last Glacial Maximum. J. Quat. Sci. 19, 335–346.

Oden, N., 1984. Assessing the significance of a spatial correlogram. Geographical Analysis 16, 116.

Petit, J. R., Jouzel, J., Raynaud, D., Barkov, N. I., Barnola, J.-M., et al., 1999. Climate and atmospheric history of the past 420, 000 years from the Vostok ice core, Antarctica. Nature 399, 429–436.

Renssen, H., Goosse, H., Fichefet, T., Campin, J., 2001. The 8.2 kyr BP event simulated by a global atmosphere sea-ice ocean model. Geophys. Res. Lett. 28, 1567–1570.

Renssen, H., Goosse, H., Muscheler, R., 2006. Coupled climate model simulation of holocene cooling events: oceanic feedback amplifies solar forcing. Clim. Past 2, 79–90.

Ricketts, R. D., Johnson, T. C., Brown, E. T., Rasmussen, K. A., Romanovsky, V. V., 2001. The Holocene paleolimnology of Lake Issyk-Kul, Kyrgyzstan: trace element and stable isotope composition of ostracodes. Paleogeogr. Palaeoclimatol. Palaeoecol. 176, 207–227.

Rimbu, N., Lohmann, G., Lorenz, S., Kim, J., Schneider, R., 2004. Holocene climate variability as derived from alkenone sea surface temperature and coupled ocean-atmosphere model experiments. Clim. Dyn. 23, 215–227.

Rodbell, D., Seltzer, G.O., Anderson, D., Abbott, M., Enfield, D., Newman, J., 1999. An 15,000-year record of El-Niño alluviation in southwestern

Ecuador. Science 283, 516–520.

Rosenthal, Y., Oppo, D. W., Linsley, B. K., 2003. The amplitude and phasing of climate change during the last deglaciation in the Sulu Sea, western equatorial Pacific. Geophys. Res. Lett. 30, 1428.

Rubensdotter, L., Rosqvist, G., 2003. The effect of geomorphological setting on Holocene lake sediment variability, northern Swedish Lapland. J. Quat. Sci. 18, 757–767.

Rühlemann, C., Mulitza, S., Lohmann, G., Paul, A., Prange, M., Wefer, G., 2004. Intermediate depth warming in the tropical Atlantic related to weakened thermohaline circulation: Combining paleoclimate data and modeling results for the last deglaciation. Palaeoceanogr. 19, 1–10,PA1025.

Sarkar, A., Ramesh, R., Somayajulu, B., Agnihotri, R., Jull, A., Burr, G., 2000. High resolution Holocene monsoon record from the eastern Arabian Sea. Earth Planet. Sci. Lett. 177, 209–218.

Sarnthein, M., van Kreveld, S., Erlenkeuser, H., Grootes, P., Kucera, M., Pflaumann, U., Schulz, M., 2003. Centennial-to-millennial-scale periodicities of Holocene climate and sediment injections off the western Barents shelf, 75N. Boreas 32, 447–461.

Schiff, C., Kaufman, D., Wolfe, A., Dodd, J., Sharp, Z., 2009. Late Holocene storm-trajectory changes inferred from the oxygen isotope composition of lake diatoms, south Alaska. Journal of Paleolimnology 41, 189–208.

Schulz, H., 1995. Meeresoberflächentemperaturen vor 10 000 Jahren – Auswirkungen des frühholozänen Insolationsmaximums. Berichte-reports, Geologisch-Paläontologischen Institut und Museum, Christian-Albrechts-Universität, Kiel.

Schulz, M., Mudelsee, M., 2002. REDFIT: Estimating red-noise spectra directly from unevenly spaced paleoclimatic time series. Comput. Geosci. 28, 421–426.

Seeberg-Elverfeldt, I. A., Lange, C. B., Arz, H. W., Pätzold, J., Pike, J., 2004. The significance of diatoms in the formation of laminated sediments of the Shaban Deep, Northern Red Sea. Mar. Geol. 209, 279–301.

Seppä, H., Birks, H., Giesecke, T., Hammarlund, D., Alenius, T., Antonsson, K., Bjune, A., Heikkilä, M., MacDonald, G., Ojala, A., et al., 2007. Spatial structure of the 8200 cal yr BP event in Northern Europe. Clim. Past 3, 225–236.

Sevellec, F., Huck, T., Jelloul, M., 2006. On the mechanism of centennial thermohaline oscillations. J. Mar. Res. 64, 355–392.

Shimada, C., Ikehara, K., Tanimura, Y., Hasegawa, S., 2004. Millennial-scale variability of Holocene hydrography in the southwestern Okhotsk Sea: diatom evidence. Holocene 14, 641–650.

Simmonds, I., Walland, D. J., 1998. Decadal and centennial variability of the southern semiannual oscillation simulated in the GFDL coupled GCM. Clim. Dyn. 14, 45–53.

Sirocko, F., 2003. What drove past teleconnections? Science 301, 1336.

Solanki, S. K., Usoskin, I. G., Kromer, B., Schüssler, M., Beer, J., 2004. Unusual activity of the sun during recent decades compared to the previous 11,000 years. Nature 431, 1084.

Sperling, M., Schmiedl, G., Hemleben, C., Emeis, K. C., Erlenkeuser, H., Grootes, P. M., Jan. 2003. Black Sea impact on the formation of eastern Mediterranean sapropel S1? Evidence from the Marmara Sea. Science 190, 9–21.

Stager, J., Cumming, B., Meeker, L., 2003. A 10,000 year high-resolution diatom record from Pilkington Bay, Lake Victoria, East Africa. Quat. Res. 59, 172–181.

Stanley, S., Deckker, P. D., 2002. A Holocene record of allochthonous, aeolian mineral grains in an Australian alpine lake; implications for the history of climate change in southeastern Australia. J. Paleolimnology 27, 207–219.

Steig, E. J., 1999. Mid-Holocene climate change. Science 286, 1485–1487.

Steig, E. J., Brook, E. J., White, J. W. C., Sucher, C. M., Bender, M. L., Lehman, S. J., Morse, D. L., Waddington, E. D., Clow, G. D., 1998. Synchronous climate changes in Antarctica and the North Atlantic. Science 282, 92–95.

Stocker, T., Wright, D., Broecker, W., 1992. The influence of high-latitude surface forcing on the global thermohaline circulation. Palaeoceanogr. 7, 529–541.

Stott, L., Cannariato, K., Thunell, R., Haug, G. H., Koutavas, A., Lund, S., 2004. Decline of surface temperature and salinity in the western tropical Pacific Ocean in the Holocene epoch. Nature 431, 56–59.

Stuiver, M., Reimer, P. J., Bard, E., Beck, J. W., Burr, G. S., Hughen, K. A., Kromer, B., McCormac, G., van der Plicht, J., Spurk, M., 1998. INTCAL98 radiocarbon age calibration, 24,000–0 cal BP. Radiocarbon 40, 1041–1083.

Sun, Y., Oppo, D., Xiang, R., Liu, W., Gao, S., 2005. Last deglaciation in the okinawa trough: Subtropical northwest pacific link to northern hemisphere and tropical climate. Palaeoceanogr. 20, 4005.

Tapia, P., Fritz, S., Baker, P., Seltzer, G., Dunbar, R., 2003. A Late Quaternary diatom record of tropical climatic history from Lake Titicaca (Peru and Bolivia). Palaeogeography Palaeoclimatology Palaeoecology 194, 139–164.

Te Raa, L., Dijkstra, H., 2003. Modes of internal thermohaline variability in a single-hemispheric ocean basin. J. Mar. Res. 61, 491–516.

Thompson, L. G., Mosley-Thompson, E., Davis, M., Henderson, P.-N. L. K., Mashiotta, T. A., et al., 2003. Tropical glacier and ice core evidence of climate change on annual to millennial time scales. Clim. Change 59, 137–155.

Thompson, L. G., Mosley-Thompson, E., Davis, M. E., Henderson, K. A., Brecher, H. H., Zagorodnov, V. S., Mashiotta, T. A., Lin, P.-N., Mikhalenko, V. N., Hardy, D. R., Beer, J., 2002. Kilimanjaro ice core records: Evidence of Holocene climate change in tropical Africa. Science 298, 589–593.

Thomson, D., 1990. Time series analysis of Holocene climate data. Phil. Trans. R. Soc. London B 330, 601–616.

van Geel, B., Heusser, C., Renssen, H., Schuurmans, C., 2000. Climatic change in Chile at around 2700 BP and global evidence for solar forcing: a hypothesis. The Holocene 10, 659.

von Grafenstein, U., Erlenkeuser, H., Müller, J., Jouzel, J., Johnsen, S., Feb. 1998. The cold event 8200 years ago documented in oxygen isotope records of precipitation in Europe and Greenland. Clim. Dyn. 14, 73–81.

Wang, L., Sarnthein, M., Erlenkeuser, H., Grimalt, J., Grootes, P., Heilig, S., Ivanova, E., Kienast, M., Pelejero, C., Pflaumann, U., 1999a. East Asian monsoon climate during the late Pleistocene: high-resolution sediment records from the South China Sea. Mar. Geol. 156, 245–284.

Wang, L., Sarnthein, M., Erlenkeuser, H., Grimalt, J., Grootes, P., Heilig, S., Ivanova, E., Kienast, M., Pelejero, C., Pflaumann, U., 1999b. East-Asian monsoon climate during the late Pleistocene: High-resolution sediment records from the South China Sea. Mar. Geol. 156, 243–282.

Wang, Y., Cheng, H., Edwards, R., He, Y., Kong, X., An, Z., Wu, J., Kelly, M., Dykoski, C., Li, X., 2005. The holocene asian monsoon: Links to solar changes and north Atlantic climate. Science 308, 854–857.

Wanner, H., Beer, J., Bütikofer, J., Crowley, T., Cubasch, U., Flückiger, J., Goosse, H., Grosjean, M., Joos, F., Kaplan, J., et al., 2008. Mid-to late holocene climate change: an overview. Quat. Sci. Rev. 27, 1791–1828.

Weber, S. L., Crowley, T. J., van der Schrier, G., 2004. Solar irradiance forcing of centennial climate variability during the Holocene. Clim. Dyn. 22, 539–553.

Weijer, W., Dijkstra, H., 2003. Multiple oscillatory modes of the global ocean circulation. J. Phys. Oceanogr. 33, 2197–2213.

Wick, L., Lemcke, G., Sturm, M., 2003a. Evidence of lateglacial and Holocene climatic change and human impact in eastern Anatolia: High-resolution pollen, charcoal, isotopic and geochemical records from the laminated sediments of Lake Van, Turkey. Holocene 13, 665–675.

Wick, L., van Leeuwen, J., van der Knaap, W., Lotter, A., 2003b. Holocene vegetation development in the catchment of Sägistalsee (1935 m asl), a small lake in the Swiss Alps. J. Paleolimnology 30, 261–272.

Witt, A., Schumann, A., 2005. Holocene climate variability on millennial scales recorded in Greenland ice cores. Nonlin. Proc. Geophys. 12, 345–352.

Xiao, J., Nakamura, T., Lu, H., Zhang, G., 2002. Holocene climate changes over the desert/loess transition of north-central China. Earth Planet. Sci. Lett. 197, 11–18.

Yu, Z., Vitt, D., Campbell, I., Apps, M., 2003. Understanding Holocene peat accumulation pattern of continental fens in western Canada. Can. J. Bot. 81, 267–282.

Yuan, D., Cheng, H., Edwards, R. L., Dykoski, C. A., Kelly, M. J., Zhang, M., et al., 2004. Timing, duration, and transitions of the last interglacial Aasian monsoon. Science 304, 575–578.

Zhang, M., Yuan, D., Lin, Y., Qin, J., Bin, L., Cheng, H., Edwards, R. L., 2004. A 6000-year high-resolution climatic record from a stalagmite in Xiangshui Cave, Guilin, China. Holocene 14, 697–702.

Zhang, X., Hegerl, G., Zwiers, F., Kenyon, J., 2005. Avoiding inhomogeneity in percentile-based indices of temperature extremes. J. Climate 18, 1641–1651.

958 **Figure captions**

Fig. 1. Global distribution of high-resolution proxy time series used in this study. Numbers refer to the 124 records (at 103 sites) and are slightly offset for better visibility. Details for each record are given in Tab. 2.

Fig. 2. Ratio of significant modes detected in a moving 4 kyr window over all 124 records to the number of modes outside the window, plotted over the center point of the time window.

Fig. 3. Two selected records: Isotopic oxygen at Sajama, Bolivia (Thompson et al., 2003) and in Soreq Cave, Israel (Bar-Matthews et al., 1999). Left: De-trended and normalized original data (black line) and treated time-series (magenta/red) for sensitivity tests (Sajama: distorted chronology, Soreq: removal of singular 8.2 and 10.8-11 kyr events). Regardless of cyclicity, all events according our definition with p_a=1.5 are marked with red triangles. Mid panel: Spectral amplitudes after applying the Lomb-Scargle transformation to the original, i.e. neither treated nor normalized record (black: total record, red: bootstrapping of upper interval, thus indicating periodicity confined to the Lower Holocene, green: Upper Holocene spectrum). Dashed vertical lines indicate significant frequencies. Right: Spectral amplitudes of treated data, either after removal of singular events or with distorted chronology.

Fig. 4. Sites with significant periodicity (red, without: blue) in the Upper and Lower Holocene. Records that show persistent modes being present in both time windows are shown as black circles. For spatial extrapolation see Methods (with half influence distance $R = 1\ 500$ km, cf. Fig. 7). (No. 3, 4 and 6 in Tab. 2 and Fig. 1).

Fig. 5. Change in periodic fluctuations from the Lower to the Upper Holocene (positive change: red, negative: blue, no significance: empty circle, significant mode without change: filled black). Blue areas indicate regions with more pronounced variability during the Lower Holocene relative to the Upper Holocene. For further explanations, see Fig. 4.

Fig. 6. Change in periodic fluctuations from the Lower to the Upper Holocene separated according spectral interval (for symbols, see Fig. 5).

Fig. 7. Spatial correlograms showing the autocorrelation (Moran's I) of mode changes plotted over the distance between sites. Values above/below the expected value of I (equal to -1/123, dotted line) can be interpreted as positive/negative correlation. From autocorrelation in N distance bins, in few cases (black filled circles) the Null-hypothesis of a random distribution can be rejected after conservative Bonferroni correction of the significance level .

Fig. 8. Mid-Holocene changes in non-cyclic frequency (number of events per millennium) around the globe. Red areas collect sites where non-cyclic frequency increased by at least 0.1 events kyr^{-1} more in the Upper compared to the Lower Holocene. In blue areas, anomaly frequency decreases by more than 0.1 events kyr^{-1}. Black dots: no or smaller change.

Figures

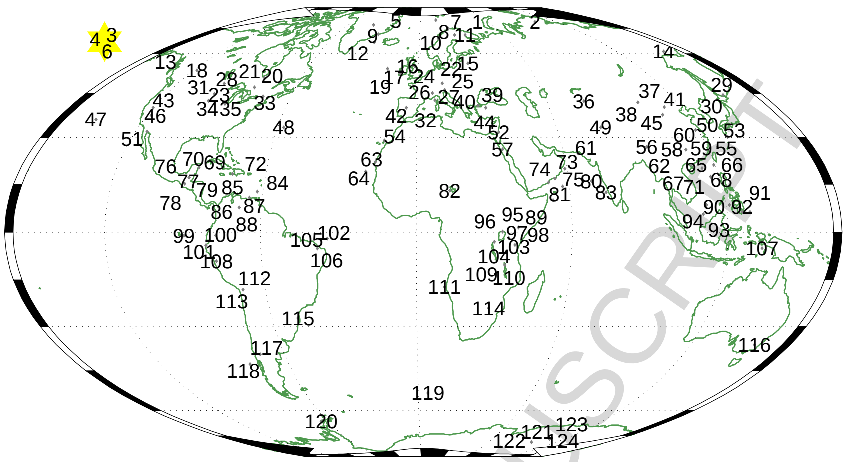

Fig. 1.

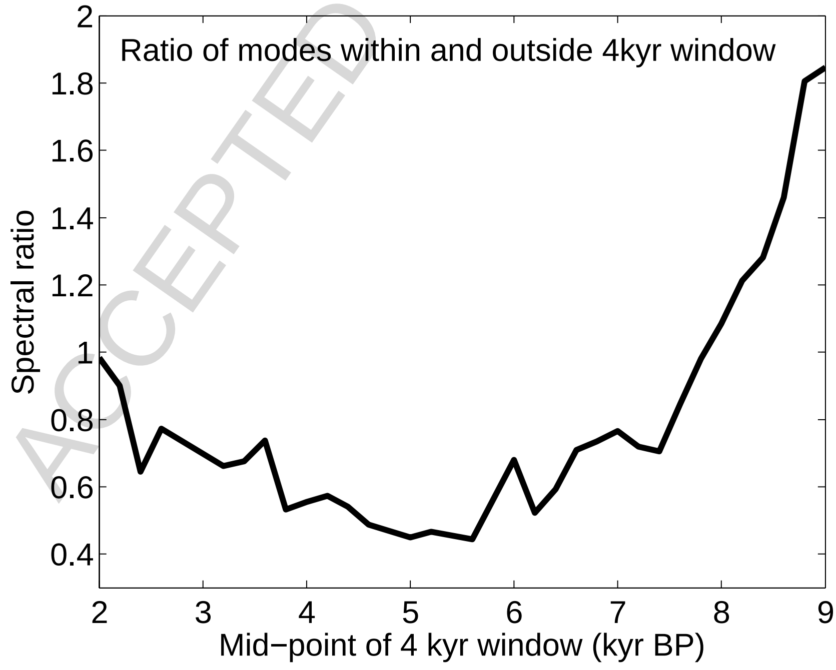

Fig. 2.

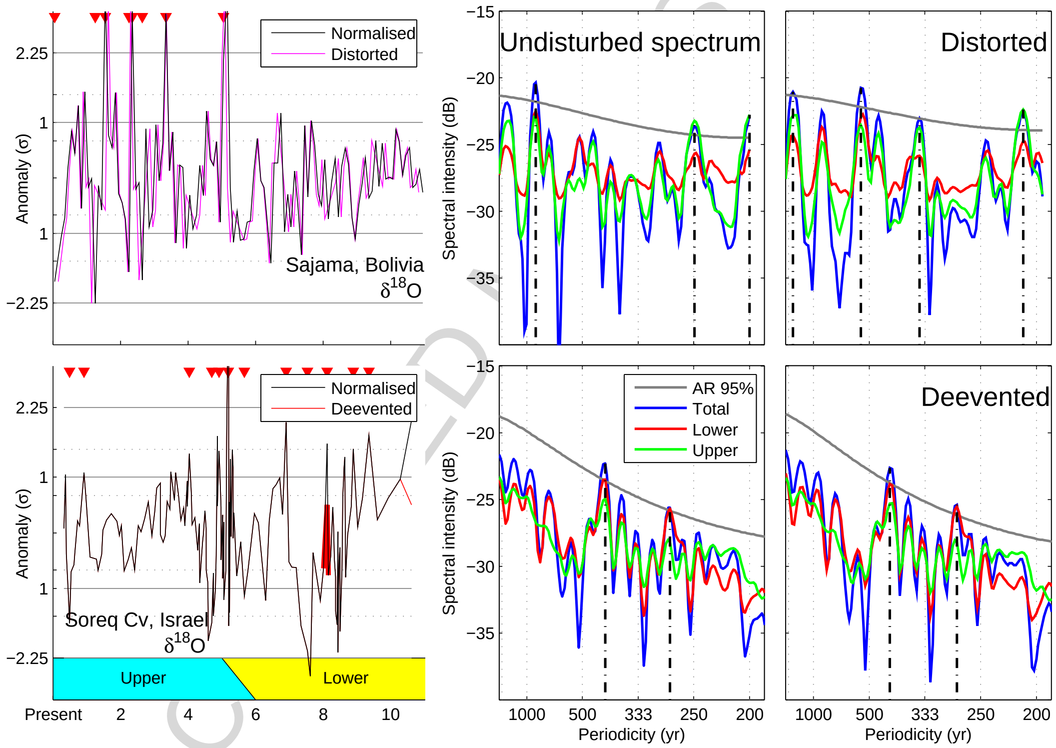
Normalised
Distorted
Anomaly (σ)
2.25
1
1
−2.25
Sajama, Bolivia
δ18O
Normalised
Deevented
Soreq Cv, Israel
δ18O
Upper
Lower
Present
2
4
6
8
10
Spectral intensity (dB)
Undisturbed spectrum
Distorted
Deevented
AR 95%
Total
Lower
Upper
−15
−20
−25
−30
−35
1000
500
333
250
200
Periodicity (yr)

Fig. 3.

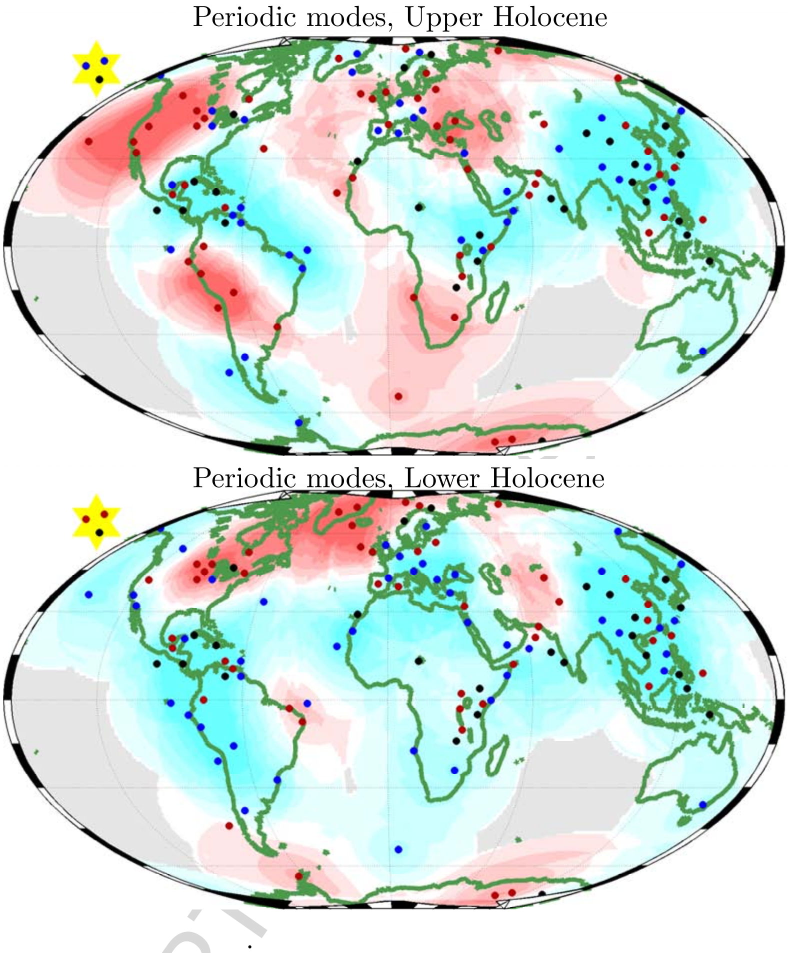
Periodic modes, Upper Holocene
Periodic modes, Lower Holocene

Fig. 4.

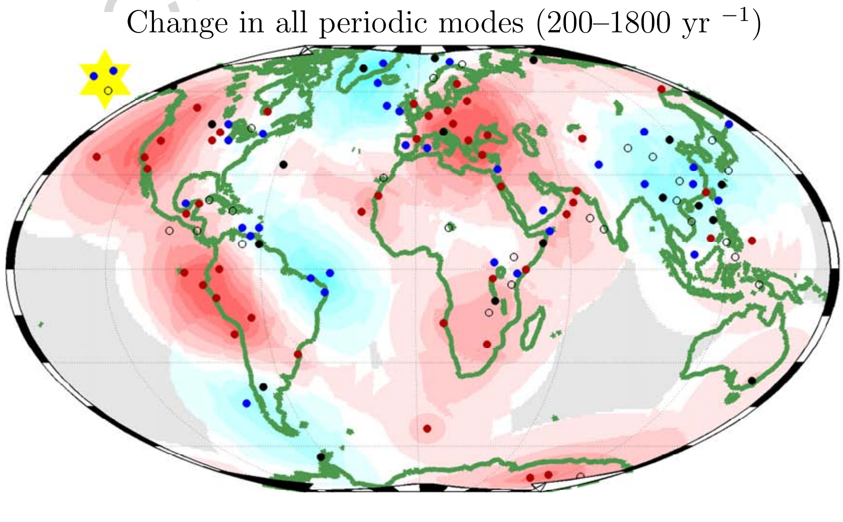
Change in all periodic modes (200–1800 yr $^{-1}$)

Fig. 5.

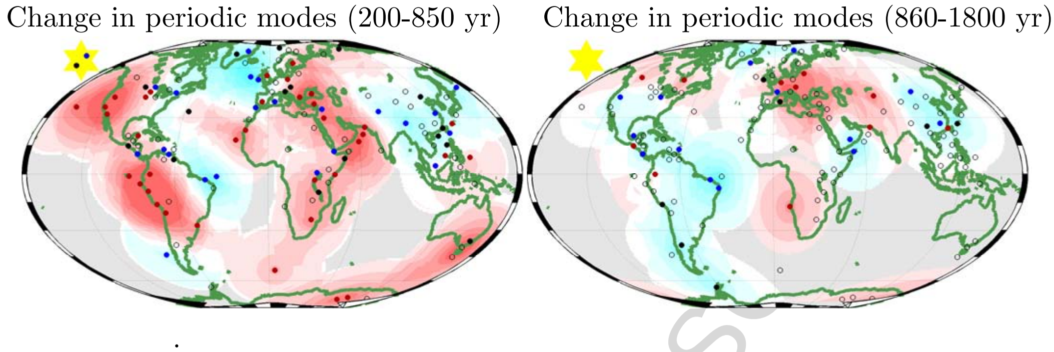
Change in periodic modes (200-850 yr)
Change in periodic modes (860-1800 yr)

Fig. 6.

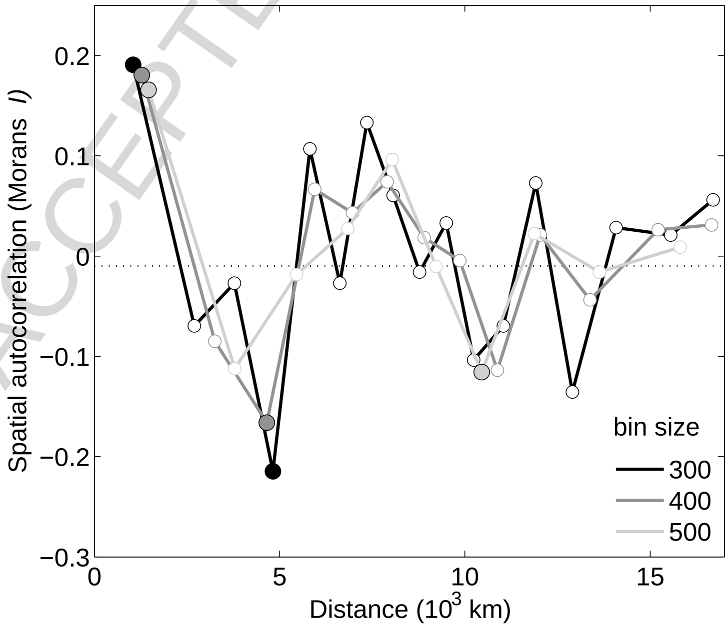
Spatial autocorrelation (Morans I)
Distance (10^3 km)
bin size
300
400
500
0.2
0.1
0
−0.1
−0.2
−0.3
0
5
10
15

Fig. 7.

Change in non-cyclic event frequency

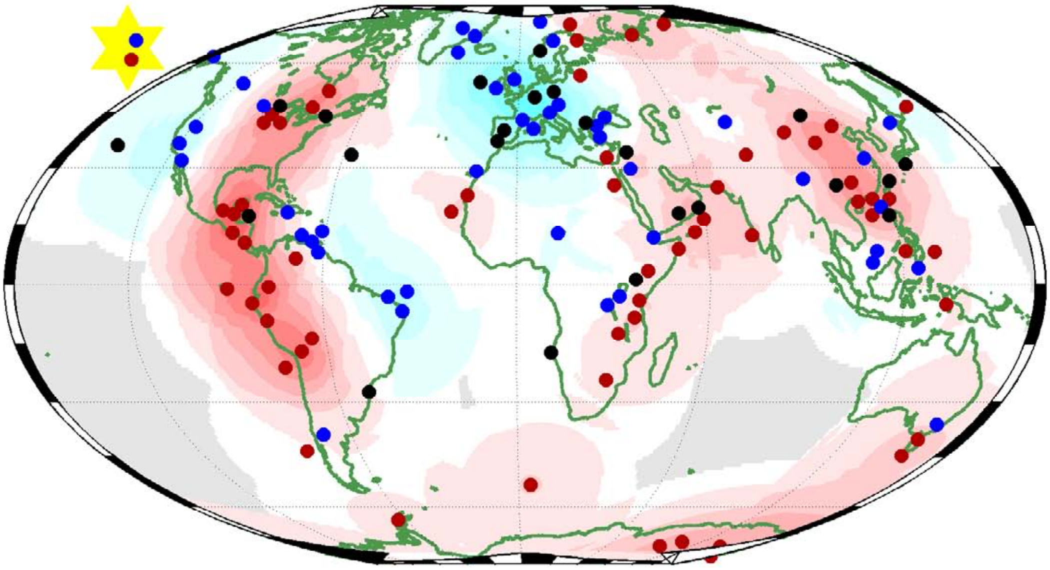

Fig. 8.

960 ## Tables

Table 1

Proxy type	Description
Isotopic oxygen fractionation $\delta^{18}O$	The interpretation of isotopic fractionation of oxygen ($\delta^{18}O$) highly depends on geographic location, environmental setting, and type of record. $\delta^{18}O$ variations in Andean glaciers and polar ice caps represent temperature. Measured in biologic deposits from closed water bodies, $\delta^{18}O$ usually indicates changes in the water balance, and thus effective moisture. However, the signal cannot be separated from temperature effects during times when the lake system is open. Speleothem $\delta^{18}O$ records the amount and composition of cave water, mostly during the wet season, and may also be influenced by temperature and above-cave lithology.
Lithic composition Mg/Ca, Charcoal, Clay, Bulk dens., Lightness, Grayscale, HSG, Lithic grains, GSD, LOI	The ratio between Mg and Ca relates to salinity (from calcium precipitation and Mg dissolution) or inorganic material input (magnesium from weathering). Wick et al. (2003a) interpret the variable Mg at constant Ca in a closed lake as changes in effective moisture, similar to the Sr/Ca ratio in ostracod shells (Ricketts et al., 2001). Grayscale density (GSD) and loss on ignition (LOI) quantify the inflow of inorganic versus organic matter. From this, cold/humid and warm/dry climates can identified but the temperature signal not separated from precipitation. The shape of grains indicates the transport process: rounded quartz grains with frequent silica coating point to aeolian import pointing to dry phases in the origin region (Stanley and Deckker, 2002). Coarse sediment layer with low organic content and many terrestrial plant macrofossils have been used by Noren et al. (2002) to find exceptional runoff events and thus storminess. Occurence of allochtonous haematite-stained grains (HSG) and icelandic glass points to ice-rafting as a consequence of increased glacier calving (e.g. Bond et al., 2001); The preservation status of aragonite at intermediate measures the bottom-water corrosiveness, and is therefore indicative for changes in the THC.
Species composition Pollen, Radiolaria, % Diatoms	Relative abundance of algal species is related to stratification and mixed layer depth and, thus, to the factor controlling both variables such as trade wind strength or freshwater increase. Pollen spectra are often taken to infer precipitation anomalies (as shaping the community structure within forests).

Table 2
Location, type, temporal coverage and reference of the climate proxy time series used in this study; the numbers in the table identify the position of proxy sites in the map (Fig. 1). Abbreviations: SS=sea surface, T=temperature, S=salinity, P=precipitation, LG=lithic grains, GSD=grayscale density, SSN=sun spot number, Lk=Lake, Cv=Cave.

No	Site	Proxy	Per	Reference	No	Site	Proxy	Per	Reference
1	N Atlantic	SST	1–11	Sarnthein et al. 2003	2	N Siberia	Pollen	0–11	Andreev et al. 2003
3	Greenland Ice	δ^{14}C	0–11	Stuiver et al. 1998	4	Greenland Ice	SSN	0–11	Solanki et al. 2004
5	Greenland Ice	δ^{18}O	0–10	Grootes and Stuiver 1997	6	Greenland Ice	Be^{10}	3–11	Finkel and Nishiizumi 1997
7	N Norway	T	1–8	Husum and Hald 2004	8	Sweden	GSD	1–11	Rubensdotter and Rosqvist 2003
9	N Atlantic	HSG	0–11	Gupta et al. 2003	10	N Finland	T	1–8	Husum and Hald 2004
11	Kola	δ^{18}O	0–9	Jones et al. 2004	12	N Atlantic	LG	1–11	Bond et al. 1997
13	NW Alaska	Mg/Ca T	0–11	Hu et al. 1998	14	Mica Lk, Alaska	Storm track	0–9	Schiff et al. 2009
15	N Atlantic	GSD	1–11	Chapman et al. 2000	16	NW Europe	ΔT	0–11	Davis et al. 2003
17	N Atlantic	HSG	0–11	Bond et al. 2001	18	W Canada	Density	0–8	Yu et al. 2003
19	Ireland	δ^{18}O	0–10	McDermott 2004	20	E Canada	Charcoal	0–8	Carcaillet et al. 2001
21	E Canada	Charcoal	0–7	Carcaillet et al. 2001	22	S Germany	δ^{18}O	0–11	von Grafenstein et al. 1998
23	Moon Lk, ND	Salinity	0–11	Laird et al. 1996	24	Lk Van, Turk.	δ^{18}O	0–11	Wick et al. 2003a
25	Swiss Alpes	T7	0–9	Wick et al. 2003b	26	Swiss Alpes	P	0–9	Wick et al. 2003b
27	C Italy	δ^{18}O	1–7	Drysdale et al. 2006	28	Sharkey, MN	Charcoal	0–11	Camill et al. 2003
29	NW Pacific	%Nitzschia	0–7	Shimada et al. 2004	30	NW Pacific	%Ozeanica	0–7	Shimada et al. 2004
31	Kimble, MN	Charcoal	0–11	Camill et al. 2003	32	C Italy	Mg/Ca T	1–7	Drysdale et al. 2006
33	New England	Storms	0–11	Noren et al. 2002	34	NC America	δ^{18}O	0–9	Denniston et al. 1999
35	Cold Water Cv, IA	δ^{18}O	0–8	Dorale et al. 1992	36	Lk Issyk-Kul, Kyrgyzstan	δ^{18}O	3–9	Ricketts et al. 2001
37	NW China	P (Ef)	2–11	Herzschuh et al. 2004	38	NW China	P (AC)	2–11	Herzschuh et al. 2004
39	Marmara Sea	$U^{k'}_{37}$ SST	0–11	Sperling et al. 2003	40	Marmara Sea	δ^{18}O	0–11	Sperling et al. 2003
41	N China	GSD	5–10	Jin et al. 2004	42	SW Europe	ΔT	0–11	Davis et al. 2003
43	Owens Lk, CA	δ^{18}O	0–11	Benson et al. 2002	44	SE Europe	ΔT	0–11	Davis et al. 2003
45	N China	Clay	0–10	Xiao et al. 2002	46	E California	P	0–8	Hughes and Graumlich 1996
47	NW Pacific	δ^{18}O	0–11	Oba and Murayama 2004	48	Bermuda Rise	δ^{18}O	1–10	Keigwin 1996
49	Tibet	δ^{18}O	0–11	Fontes et al. 1996	50	Dongge Cv, China	δ^{18}O	0–11	Yuan et al. 2004
51	S California	Moisture	0–7	Davis 1992	52	Soreq Cv, Israel	δ^{18}O	0–11	Bar-Matthews et al. 1999
53	E China Sea	SST	0–11	Fengming et al. 2008	54	Canary	δ^{18}O	0–11	Freudenthal et al. 2002
55	E China Sea	SST	1–11	Sun et al. 2005	56	Dunde, China	δ^{18}O	0–9	Jung et al. 2004
57	Red Sea	δ^{18}O	1–11	Seeberg-Elverfeldt et al. 2004	58	Xiangshui Cv, China	δ^{18}O	0–6	Zhang et al. 2004
59	Dongge Cv, China	P	0–11	Dykoski et al. 2005	60	Dongge Cv, China	δ^{18}O	0–9	Wang et al. 2005

61	NE Arabian Sea	δ^{18}O	0–11	Doose-Rolinski et al. 2001	62	S China	Moisture	0–10	Liu et al. 2000
63	Trop Atlantic	δ^{18}O	0–11	Knaack 1997	64	Trop Atlantic	SST	0–11	deMenocal et al. 2000
65	S China Sea	δ^{18}O	0–11	Wang et al. 1999a	66	S China Sea	SSS	0–9	Jung et al. 2004
67	S China Sea	Silt	0–11	Wang et al. 1999a	68	S China Sea	δ^{18}O	0–11	Wang et al. 1999b
69	Yucatan	δ^{18}O (Ph)	0–8	Hodell et al. 1995	70	Yucatan	δ^{18}O (Py)	0–8	Hodell et al. 1995
71	Taiwan	LOI	2–11	Huang et al. 1997	72	Haiti	δ^{18}O	0–10	Higuera-Gundy et al. 1999
73	Arabian Sea	δ^{18}O	0–11	Gupta et al. 2003	74	Oman	δ^{18}O	3–8	Fleitmann et al. 2003
75	Qunf Cv, Oman	δ^{18}O	0–11	Fleitmann et al. 2007	76	Yucatan	δ^{18}O	0–8	Curtis et al. 1996
77	Guatemala	δ^{18}O (Py)	0–9	Curtis et al. 1998	78	Guatemala	δ^{18}O (Co)	0–9	Curtis et al. 1998
79	Guatemala	δ^{18}O (Cy)	0–8	Curtis et al. 1998	80	Peru	P (diatom)	0–11	Tapia et al. 2003
81	Arabian Sea	SSTW	0–11	Schulz 1995	82	Sahel	δ^{18}O	0–11	Gasse 2002
83	E Arabian Sea	δ^{18}O	0–10	Sarkar et al. 2000	84	NE Canada	GSD	4–9	Barber et al. 1999
85	Cariaco Basin	SST	0–11	Lea et al. 2003	86	Cariaco Basin	Titanium	0–11	Haug et al. 2001
87	Cariaco Basin	GSD	0–11	Haug et al. 2001	88	Venezuela	δ^{18}O	0–8	Curtis et al. 1999
89	Somalia	δ^{18}O	0–10	Jung et al. 2004	90	S China Sea	δ^{18}O	0–11	Wang et al. 1999a
91	Sulu Sea	δ^{18}O	4–11	Rosenthal et al. 2003	92	W Pacific	δ^{18}O (81)	0–11	Stott et al. 2004
93	W Pacific	δ^{18}O	0–11	Rosenthal et al. 2003	94	S China Sea	δ^{18}O	3–11	Kienast et al. 2001
95	Lk Victoria	Diatoms	0–10	Stager et al. 2003	96	Lk Victoria	Diatoms	0–10	Stager et al. 2003
97	Lk Hall, Kenia	δ^{18}O	1–11	Barker et al. 2001	98	Lk Sim, Kenia	δ^{18}O	1–10	Barker et al. 2001
99	E Pacific	δ^{18}O	2–11	Rosenthal et al. 2003	100	Ecuador	GSD	0–11	Rodbell et al. 1999
101	Ecuador	ENSO	0–10	Moy et al. 2002	102	Eq Atlantic	ΔSST	0–11	Kim and Schneider 2003
103	Burundi	P	0–11	Bonnefille and Chalie 2000	104	Kilimanjaro	δ^{18}O	0–11	Thompson et al. 2002
105	W Atlantic	δ^{18}O	0–11	Arz et al. 2001	106	W Atlantic	δ^{18}O (Tu)	0–11	Arz et al. 2001
107	W Pacific	δ^{18}O (76)	0–11	Stott et al. 2004	108	Huascaran, Peru	δ^{18}O	0–11	Thompson et al. 2003
109	Lk Malawi	MAR	0–11	Johnson et al. 2002	110	Lk Malawi	Si	0–11	Johnson et al. 2002
111	Angola Basin	$U^{k'}_{37}$SST	0–11	Kim and Schneider 2003	112	Sajama, Bolivia	Particles	0–11	Thompson et al. 2003
113	Sajama, Bolivia	δ^{18}O	0–11	Thompson et al. 2003	114	SE Africa	δ^{18}O	0–10	Holmgren et al. 2003
115	Botuvera Cv, Brasil	δ^{18}O	0–11	Cruz et al. 2005	116	SW Australia	Particles	1–11	Stanley and Deckker 2002
117	Chilean Coast	SST	0–8	Lamy et al. 2001	118	Chile	δ^{18}O	0–8	Lamy et al. 2002
119	S Atlantic	LG	0–10	Hodell et al. 2001a	120	W Antarctic	Inclination	1–9	Brachfeld et al. 2000
121	Vostok, Antarctica	δ^{2}H	0–11	Petit et al. 1999	122	Komsomolskaia	δ^{2}H	0–11	Masson et al. 2000
123	Taylor dome	δ^{18}O	0–11	Grootes et al. 1994	124	Taylor dome	δ^{2}H	0–11	Steig et al. 1998